At what frequencies should air-core magnetics be used?

Michael Solomentsev, Alex J. Hanson
University of Texas at Austin
2501 Speedway, Austin, TX 78712, USA
mys432@utexas.edu, ajhanson@utexas.edu

***Abstract*—Magnetic components for power conversion (inductors & transformers) are often designed with magnetic cores, which add core loss but reduce the required number of turns, copper loss, and usually total loss. At very high frequencies, poor core materials make this tradeoff less advantageous and air-core magnetic components are often preferred. The boundary between the magnetic-core and air-core regimes has not yet been theoretically identified, and intermediate frequency ranges (i.e. 5 to 30 MHz) see both cored and air-core examples. In this work, we calculate an expression that suggests that, based on the properties of currently available magnetic materials, cored inductors can outperform their air-core counterparts up to 60 MHz, well into the VHF range. We experimentally demonstrate this boundary frequency by comparing the quality factors of optimized cored and air-core toroidal inductors. Formally demonstrating the advantage of cored over air-core inductors even at tens of MHz suggests more advantageous designs for applications at ISM bands (6.78, 13.56, 27.12 MHz) and other RF applications.**

***Index Terms*—High Frequency Magnetics, Performance Factor, Core Loss, Copper Loss**

I. Introduction

As power converters are more frequently being designed to operate using switching frequencies in the megahertz range, careful design of magnetic components is necessary to prevent excess loss. Typically, magnetic components are designed to have cores to reduce the required number of turns to achieve a given inductance and energy storage. The core does introduce core loss, but the tradeoff is usually advantageous at conventional power conversion frequencies (approximately 10 kHz to 1 MHz).

Both core and copper losses scale with frequency: the former due to micro- and macro-scopic eddy currents in the core, and the latter due to the appearance of eddy currents in the windings at moderate frequencies and shrinking skin depths as frequency increases. While skin depth decreases proportional to $f^{\frac{1}{2}}$ (and thus copper loss scales up at that rate), core loss increases at a rate of f^{α} [1]–[3], where α is a material parameter with typical values between 1 and 2. Managing core loss requires more turns and larger gaps at higher frequency. For very high frequencies, it is both theoretically advantageous and practically convenient to design magnetic components with no core at all. Air-core magnetics are common in applications above approximately 5 MHz [4]–[8].

A more quantitative way to express the suitability of magnetic cores for operation at a particular frequency is with the performance factor $\mathcal{F} = f\hat{B}$, with units of mT·MHz. The performance factor is a material figure of merit that expresses the maximum B field $\hat{B}$ that can be imposed on a given material at a given frequency f before reaching a predefined core loss density (typically chosen between 200 and 500 mW/cm^3). It has been shown that the achievable power handling capability of a magnetic component is proportional to the performance factor or minor modifications to it [9]. While the performance factor may be useful in comparing the relative suitability of core materials for operation at a frequency, it does not directly provide a way to compare the use of these materials to an air-core structure. Nevertheless, it has been shown that several NiZn materials have good performance factors at tens of MHz [9], [10], suggesting that cored inductors may still be suitable for use at higher frequencies where air-core magnetics currently dominate.

Air-core structures dominate in the 5 to 50 MHz space, across a variety of applications. Converters are regularly designed to implement wireless power transfer for medical devices at the 6.78 MHz, 13.56 MHz, and occasionally 27.12 MHz. While this application space regularly requires the use of core-less structures for the transfer and receiver coils when operating in the MHz range (although wireless power transfer implementations in the kHz range regularly use backplate cores), matching networks with inductive elements are often necessary. Implementations of such matching networks predominantly rely on air-core inductors in their designs [11]–[15]. Moreover, high-frequency power inverters and their associated matching networks are used for plasma generation (necessary for semiconductor manufacturing, RF heating for food applications [16], among others) and particle acceleration [17], [18]. Such converters operate well into the tens of MHz and again predominantly use air-core components. Less application-oriented research has developed high-frequency resonant inverters that operate at 27.12 MHz [19], [20], 30 MHz [21], and up to 40.68MHz [22]; examples which all utilize air-core components.

Some relatively recent examples of cored magnetics in the HF regime signal the potential for cored magnetics in this frequency domain. [23] uses a magnetic core for a 13.56 MHz ac inductor and achieves much higher quality factor than its air-core counterparts. [24] develops very high Q self-resonant magnetics for wireless power transfer at 6.78 MHz. These exceptions anecdotally suggest what this paper

intends to formally demonstrate: that cored magnetics may be superior (per unit volume) in many applications where air-core components are currently favored.

In this work, we calculate an expression that represents the crossover point where air-core inductors outperform their cored counterparts. The result can be expressed in terms of performance factor and indicates that the crossover point occurs at a very low value of $\mathcal{F}$, which is exceeded by commercially-available materials up to approximately 60 MHz. We validate this by designing cored and air-core inductors optimized for a certain volume, target impedance, and frequency. We then measure the quality factor of these inductors and find higher performance in the cored structures up to approximately 60 MHz.

II. Theoretical Derivation Based on Constant $\hat{J}$ & $\hat{B}$

A. Derivation 1: Comparing Power Processing Capability

One potential method for identifying the threshold where air-core structures outperform cored structures is by comparing each of their power processing capabilities. Consider specifically two inductors with toroidal geometries where the available conduction area is limited by the skin depth, shown in Fig. 1, one with a magnetic core and one with an air core (the toroidal geometry is chosen so that the flux distribution is not severely different between the core and air-core cases). Further assume in both cases that there are certain limitations on maximum loss density, determined either by converter efficiency requirements or heating constraints. These manifest in a maximum peak AC flux density $\hat{B}$ based on a *core loss density limit* and a maximum current density $\hat{J}$ based on a *copper loss density limit*, $P_{cu,V}$. The maximum voltage that can be applied to the component is given by Faraday's law and the flux density limit: $V_{max} = N\frac{d\phi}{dt} = NA_c\hat{B}\omega\cos\omega t$. Using the current density limit, $\hat{J}$, calculate a peak current in the cored inductor, $I_{max} = \hat{J}\delta l_c/N$. This produces a maximum power handling capability for a cored inductor:

$$P_{cored} = \frac{1}{2}I_{max}V_{max} = \frac{1}{2}(NA_c\hat{B}\omega)\frac{\hat{J}\delta l_c}{N} = \frac{1}{2}A_c l_c \delta \hat{B}\hat{J}\omega \tag{1}$$

The above expression is calculated in [9] in the derivation of both the standard performance factor ($\mathcal{F} = \hat{B}f$) and modified performance factors (including $\mathcal{F}_{3/4} = \hat{B}f^{\frac{3}{4}}$).

We now make a similar calculation for an air-core inductor. In the air-core case, voltage is not constrained by B field (because there is no core loss), but by inductance (i.e. $v = L\frac{di}{dt}$):

$$V = LI\omega = \frac{N^2}{\mathcal{R}}I\omega = \frac{N^2A_c\mu_0}{l_c}I\omega \tag{2}$$

The peak current is the same as in the cored case. Then, we extract a maximum air-core power handling capability:

$$P_{air-core} = \frac{1}{2}IV = \frac{N^2A_c\mu_0}{2l_c}(\frac{\hat{J}\delta l_c}{N})^2\omega = \frac{1}{2}\mu_0 A_c l_c \hat{J}^2\delta^2\omega = \rho A_c l_c \hat{J}^2 \tag{3}$$

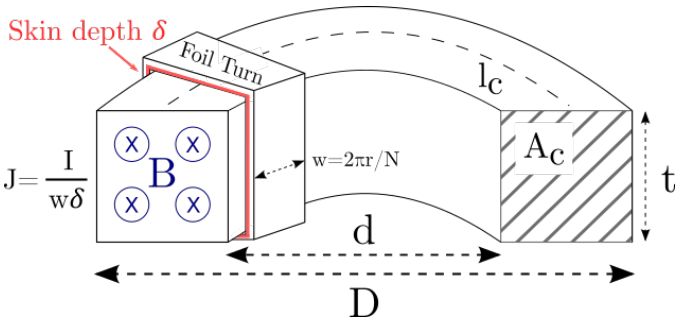

Fig. 1: Labeled geometry of a toroid cross-section.

where that the skin depth is given by $\delta = \sqrt{\frac{2\rho}{\omega\mu_0}}$. Comparing the power processing capability of both inductors yields:

$$\frac{P_{cored}}{P_{air-core}} = \frac{\frac{1}{2}A_c l_c \delta \hat{B}\hat{J}\omega}{\rho A_c l_c \hat{J}^2} = \frac{\delta\hat{B}\omega}{2\rho\hat{J}} = \frac{\pi\delta\hat{B}f}{\rho\hat{J}} = \frac{\pi\delta\mathcal{F}}{\rho\hat{J}} \tag{4}$$

When the above expression is equal to 1, the power processing capability of two equivalently sized core & air-core inductors is equal, given the same loss density constraints. Note the use of the conventional performance factor, $\mathcal{F} = \hat{B}f$. Thus, (4) can be used to identify a threshold, in terms of frequency or performance factor, where it becomes more advantageous to use no core:

$$1 \leq \frac{\pi\delta\mathcal{F}}{\rho\hat{J}} = \frac{\pi\mathcal{F}}{\rho\hat{J}}\sqrt{\frac{2\rho}{\omega\mu_0}} = \frac{\pi\mathcal{F}}{\hat{J}\sqrt{\frac{1}{2}\rho\omega\mu_0}} = \frac{\pi\mathcal{F}}{\sqrt{\frac{1}{2}P_{cu,V}\omega\mu_0}} \tag{5}$$

$$\frac{\mathcal{F}}{\sqrt{f}} = \mathcal{F}^{\frac{1}{2}} \geq \sqrt{\frac{\mu_0 P_{cu,V}}{\pi}} \quad \text{for } \frac{P_{core}}{P_{air}} = 1 \tag{6}$$

where $\mathcal{F}^{\frac{1}{2}}$ is a modified performance factor which has been used in other contexts to account for high-frequency copper loss effects, as described in [9]. Further discussion of this expression and its significance will be presented in Section III.

B. Derivation 2: When Required l_g Equals l_c

This same expression can be calculated through an alternative method. Consider the design of a cored inductor with an air gap. When using a sufficiently high-permeability core, inductance will be almost entirely determined by the length of the air gap (as opposed to the length of the core). As frequency increases, the required gap length to maintain constant core loss density in the core increases as well (the allowed B field, $\hat{B}$, decreases with frequency). The cross-over point where air-core components are more advantageous (for a given volume) occurs when the calculated gap length reaches total core length. Begin by establishing a target inductance:

$$L = \frac{N^2}{\mathcal{R}} = \frac{N^2\mu_0 A_c}{l_g} = \frac{N^2\mu_0 A_c}{l_c} \tag{7}$$

Just as before, the inductor has limits on maximum B field and current density, set by loss density requirements. These limitations will constrain the turn count and current: $N = l_g\hat{B}/\mu_0 I$. Then substitute this requirement into the expression for inductance:

$$L = \frac{\mu_0 A_c l_g^2 \hat{B}^2}{\mu_0^2 l_g I^2} = \frac{A_c l_g \hat{B}^2}{\mu_0 I^2} = \frac{A_c l_g (\hat{B}f)^2}{\mu_0 f^2 I^2} = \frac{A_c l_g \mathcal{F}^2}{\mu_0 f^2 I^2} \quad (8)$$

After moving the inductance over to the right hand side of the expression, it can be further simplified by noting that N^2 is proportional to inductance, and eliminating the remaining dimensional quantities. Converting to inequality and isolating performance factor produces the same result as the derivation presented in Section II-A.

$$1 = \frac{A_c l_g \mathcal{F}^2}{\mu_0 L f^2 \frac{\hat{J}\delta l_g}{N}^2} = \frac{\pi A_c \mathcal{F}^2}{\rho l_g f \hat{J}^2} \frac{N^2 \mathcal{R}}{N^2} = \frac{\pi A_c \mathcal{F}^2}{\rho l_g f \hat{J}^2} \frac{l_g}{\mu_0 A_c} \quad (9)$$

$$\frac{\mathcal{F}}{\sqrt{f}} = \mathcal{F}^{\frac{1}{2}} \geq \sqrt{\frac{\mu_0 \rho \hat{J}^2}{\pi}} = \sqrt{\frac{\mu_0 P_{cu,V}}{\pi}} \quad (10)$$

$$\text{for } \frac{P_{core}}{P_{air}} = 1$$

C. Analysis

Equation (6) expresses the performance factor threshold in terms of a copper loss density. If we assume the allowable copper loss density for the air-core structure is the same as that of a cored inductor, e.g. $P_{cu,V} = 200$ mW/cm^3, the expression yields $\mathcal{F}^{\frac{1}{2}} = .282$ mT·MHz$^{1/2}$. Material performance factors sit well above this constraint at frequencies with available data. Projecting out a trend line based on the existing envelope of performance factors suggests an intersection in the hundreds of MHz, as shown in Fig. 2. Note that the calculated result is dependent on the parameter $P_{cu,v}$, but the square-root dependence is weak and the resulting performance factor value is very small, so the qualitative conclusion and the estimate of crossover frequency remain strong.

III. Theoretical Derivation Based on Constant Total Loss

A. Derivation

The previous section's analysis followed from assumptions that core and copper loss densities should be held constant. It may be more advantageous to consider alternative constraints, as optimized magnetic components near the boundary frequency will have a small fraction of the core volume occupied with magnetic material. The core's contribution to the overall thermal environment is therefore small and more conduction loss could be tolerated. One alternative constraint would be to hold total loss density constant. If thermal constraints would ordinarily allow a certain loss density in the core and in the copper, then the small-core-volume case can be calculated by generating a new allowable loss density, P'_V:

$$P_{total} = P_{core,V} Vol_{core} + P_{cu,V} Vol_{cu} \quad (11)$$

$$P'_V = \frac{1}{Vol_{cu}} (P_{core,V} Vol_{core} + P_{cu,V} Vol_{cu}) \quad (12)$$

For a a toroidal structure with outer diameter D, inner diameter d, and core thickness t, $Vol_{core} = \pi t \frac{1}{4}(D^2 - d^2)$ and $Vol_{cu} = \frac{\pi\delta}{2}(D^2 - d^2)$ (note that this assumes the entire surface area of the toroid will be used for conduction). This produces a ratio of: $Vol_{core}/Vol_{cu} = t/2\delta$. Calculating the new allowable loss density and substituting it into Equation 6 produces a new expression for the air-core threshold:

$$P'_V = \frac{t}{2\delta} P_{core,V} + P_{cu,V} \approx P_V (\frac{t}{2\delta} + 1) \approx \frac{t}{2\delta} P_V \quad (13)$$

$$\mathcal{F} = \sqrt{\frac{\mu_0 t f P_V}{2\pi \sqrt{\frac{\rho}{\pi \mu_0 f}}}} = \frac{\mu_0^{\frac{3}{4}} P_V^{\frac{1}{2}} t^{\frac{1}{2}} f^{\frac{3}{4}}}{\sqrt{2}\pi^{\frac{1}{4}} \rho^{\frac{1}{4}}} = \sqrt[4]{\frac{\mu_0^3 P_V^2 t^2 f^3}{4\pi\rho}} \quad (14)$$

$$\text{for } \frac{P_{core}}{P_{air}} = 1$$

Equation (14) can also be expressed in terms of $\mathcal{F}_{1/2}$ as was done previously:

$$\mathcal{F}_{1/2} = \frac{\mu_0^{\frac{3}{4}} P_V^{\frac{1}{2}} t^{\frac{1}{2}} f^{\frac{1}{4}}}{\sqrt{2}\pi^{\frac{1}{4}} \rho^{\frac{1}{4}}} \quad (15)$$

where the exponent of frequency is reduced to $1/4$. (15) may also prompt us to define another modified performance factor, $\mathcal{F}_{1/4} = \hat{B} f^{1/4} = \mathcal{F}/f^{3/4}$ in order to create a metric that is not explicitly a function of frequency.

$$\mathcal{F}_{1/4} = \frac{\mu_0^{\frac{3}{4}} P_V^{\frac{1}{2}} t^{\frac{1}{2}}}{\sqrt{2}\pi^{\frac{1}{4}} \rho^{\frac{1}{4}}} \quad (16)$$

B. Analysis

For a P_V of 200 mW/cm^3 and a t of 10 mm, the core/air-core threshold comes out as: $\mathcal{F}_{\frac{1}{4}} = 2.47$ mT·MHz$^{1/4}$; $\mathcal{F}_{\frac{1}{2}} = 2.47 f^{\frac{1}{4}}$ mT·MHz$^{1/2}$; $\mathcal{F} = 2.47 f^{\frac{3}{4}}$ mT·MHz. Both this threshold and the one calculated using the constant $P_{cu,V}$ assumption are plotted on Fig. 2. Note that this threshold is relatively insensitive (square-root dependence) to the toroid thickness t and the original choice of loss density P_V, and would therefore apply well to a variety of design scenarios.

Figures 2 and 3 show a selection of modified performance factors of magnetic materials designed for high-frequency operation (the various performance factors represent the same data, just in slightly different ways). Note that while the envelope of these performance factors decays with frequency, many materials sit higher than both calculated thresholds for air-core advantage well into the tens of MHz. Projecting out a trend line based on the envelope of best-performing materials, the crossover point does not appear to be reached until the hundreds of MHz when B and J are individually constrained, or approximately $60\,\mathrm{MHz}$ when total loss density is constrained. Many published designs in the 5-50 MHz space use air-core components, but this analysis suggests that cored structures would reduce loss further in the same volume, as in [23], [25]. Cored structures may also reduce the fields exterior to the magnetic structure, reducing EMI, loss, and the need for

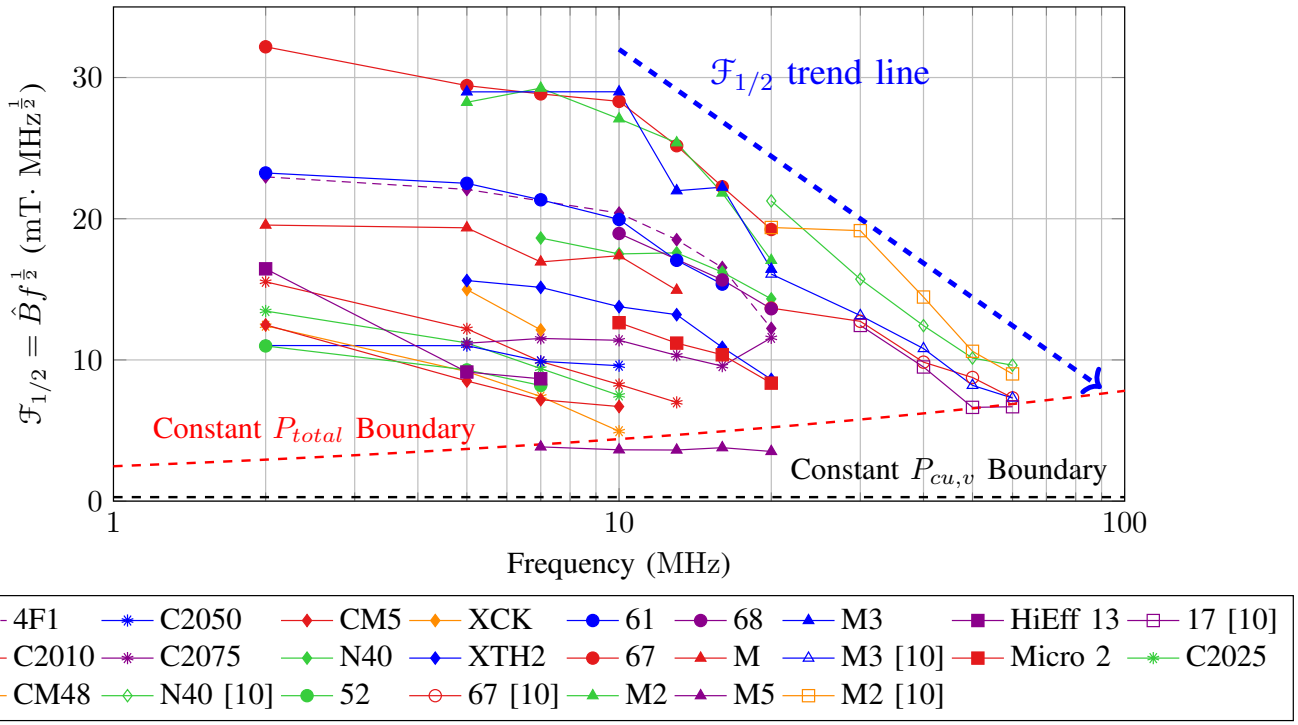

Fig. 2: Survey of $\mathcal{F}_{1/2}$ [9]. Dashed lines show the envelope of modified performance factor as frequency increases (in blue) the calculated crossover point for $P_V = 200$ mW/cm^3 and core thickness of 10 mm (in black and red).

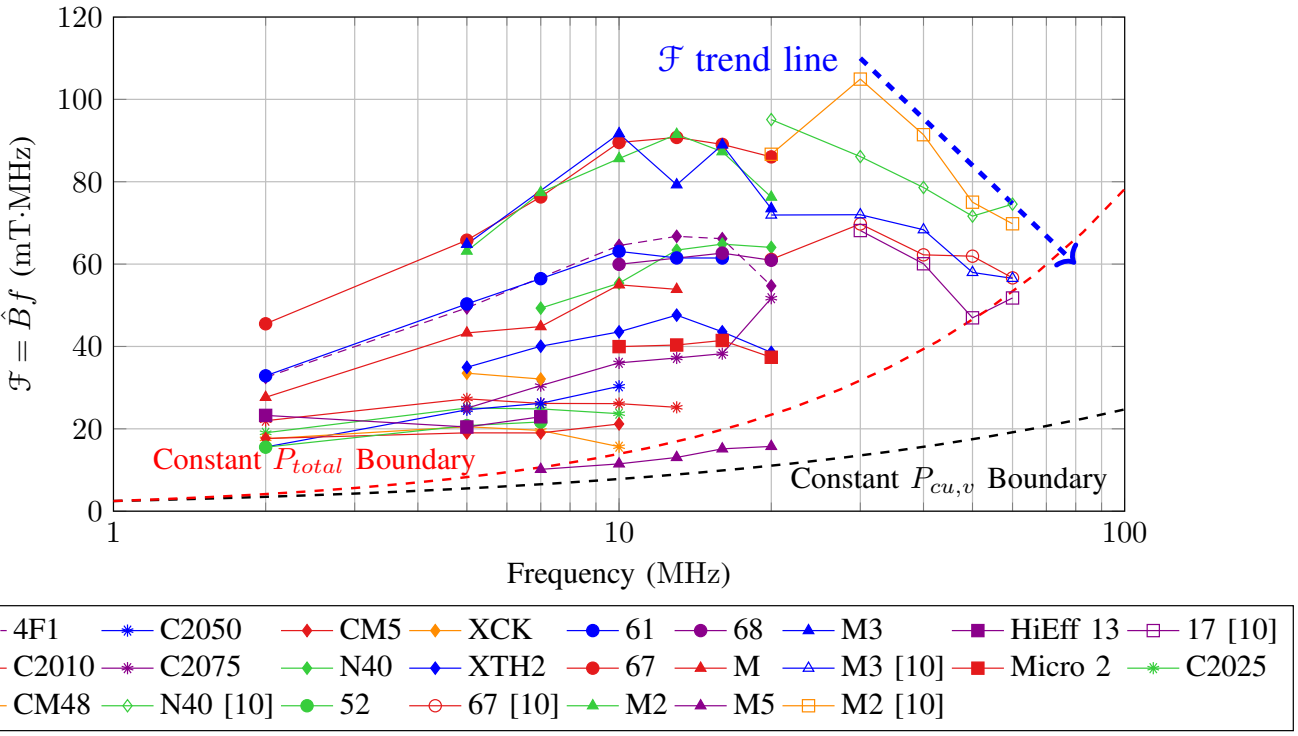

Fig. 3: Survey of $\mathcal{F}$ [9]. Dashed lines show the envelope of modified performance factor as frequency increases (in blue) the calculated crossover point for $P_V = 200$ mW/cm^3 and core thickness of 10 mm (in black and red).

shielding [26].

IV. Experimental Verification

To validate (6) and (14), several pairs of cored and air-core high-frequency inductors were built. Each pair was designed to have the same volume, operating frequency, power loss density, and target impedance. We used toroidal cores as outlined in our analysis above. Each inductor was optimized for high performance in order to make the comparison fair. The optimization process is described in Appendix A.

Based on the data shown in Figure 2, a magnetic material best suited for each operating frequency was chosen: Fair-Rite 67 for 10 MHz; National Magnetics Group M2 for 30 MHz; and NMG N40 for 60 MHz. Single frequency operation and full utilization of core surface area using foil windings (or standard magnet wire, depending on the turn count and toroid size) were assumed. By calculating copper and core loss for each case, optimized core designs were produced for a total loss density of 200 mW/cm^3. This method produced optimized designs specifying the percent of the toroid that should be magnetic material, ensuring constant volume. Note that while our analysis assumed the use of foil windings to maximize conduction area, our final wound inductors utilized traditional round magnet wire – this design choice is justified in Appendix B.

While the percentage of core to total volume was high in the 10 MHz case (91% to 98%, depending on the core), it was significantly smaller in the 30 MHz (75% to 86%) and 60 MHz (45% to 56%) cases. This required the use of quasi-distributed gaps [27] to minimize fringing flux and ensure the accuracy of the optimization. Intact toroids were sliced into smaller pieces using a 3400 RPM diamond lapidary saw, then taped or glued together with appropriately sized gaps. Figure 5 shows a selection of cores across different frequencies: the 67 core has two gaps, the M2 core has four, and the N40 core is constructed from eight pieces of a core sliced into 16ths, then assembled using a 3D printed jig. Using the volume of the cored toroid as a fixed target in each case, a similar optimization script for air-core structures was run. Unconstrained by core dimensions, we varied both the toroid's cross-sectional radius and its axial radius while keeping total cylindrical volume constant, varying turn count to achieve target impedance. This again led us to an optimized design for a particular power loss density in each case. These specifications were used to create 3D models, which were then 3D-printed and windings were wound around the resulting "core" shape.

The quality factor of the inductors was then measured using a series resonant testing setup, described in Appendix C. Each inductor was tested at its operating frequency and a variety of drive currents, corresponding to various power loss densities. Small-signal quality factors for the air-core inductors were also collected using an E5061B impedance analyzer (with 3 GHz bandwidth) to validate the testing rig; the results match well with our experimental measurements, which indicates that the series resonant approach was valid.

The results are shown in Figure 4. In both the 10 and 30 MHz cases, core materials significantly outperform their air-core counterparts, by factors of roughly 3.5 and 1.7 respectively for the 100 Ω inductors. At 60 MHz, where (14) indicates that an N40 core inductor should narrowly outperform an air-core counterpart, experimental data indicates the air-core structure had roughly 20% larger Q than the cored inductor.

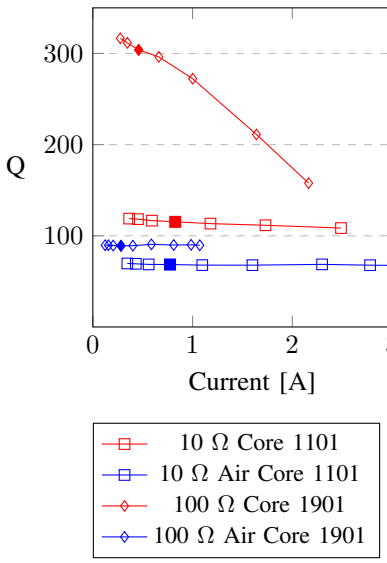

(a) Optimized Fair-Rite 67 and air-core inductors operating at 10 MHz

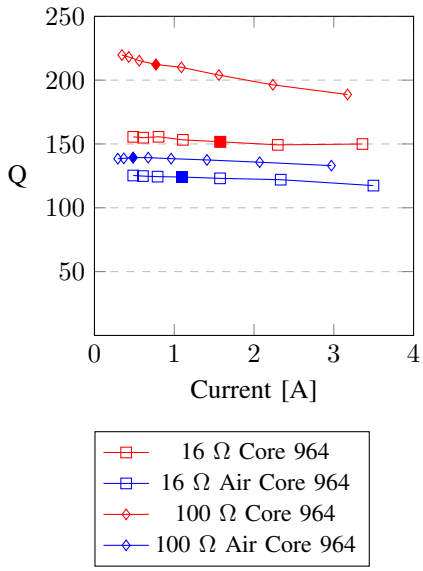

(b) Optimized M2 and air-core inductors operating at 30 MHz

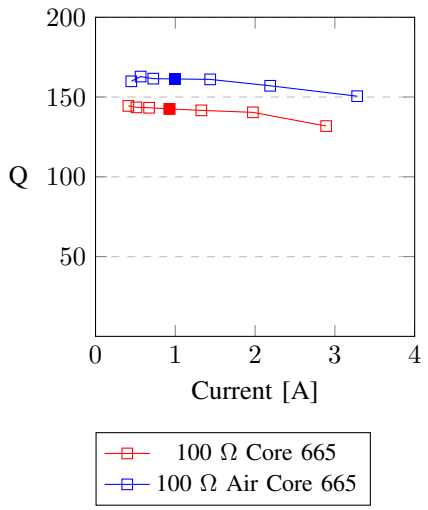

(c) Optimized N40 and air-core inductors operating at 60 MHz

Fig. 4: Experimental Q measurements plotted against drive current at various frequencies, showing substantially higher performance from cored inductors at 10 and 30 MHz. The filled in data points correspond to approximately $P_v = 200$ mW/cm^3.

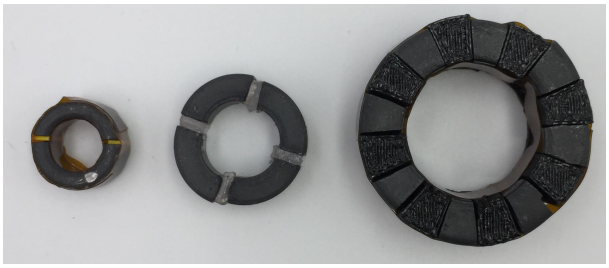

Fig. 5: Unwound toroidal cores showing implementation of quasi-distributed gaps for 10, 30, and 60 MHz.

We note that the 60 MHz core had an extremely large air gap which required repeated core slicing to produce many still-large air gaps, along with various other non-idealities which made it stray from our ideal derivation. Its competitiveness with the air-core version at 60 MHz further indicates the potential of cored structures in high frequency applications.

V. Conclusion

While high frequency power converters typically rely on air-core magnetic components to avoid disproportionately large core loss, the region of validity of this design choice is not well understood, potentially leaving available performance on the table in applications operating at frequencies of about 5-50 MHz. In this work, we derive a formal expression that indicates the frequency at which air-core magnetic components supersede their cored counterparts for a given volume (a calculation based on equal weight would favor air-core components at even lower frequencies). This boundary depends largely on the performance factor of the magnetic cores in question. Based on the performance factors of commercially available magnetic cores, air-core inductors only eclipse cored inductors well into the VHF regime, at around 60 MHz. We validate this conclusion by building a series of cored and air-core inductors optimized at 10, 30, and 60 MHz with identical impedance and volume. By measuring the quality factor of these inductors, we show agreement with our theoretical derivation and show higher performance of cored structures in the 10s of MHz. Importantly, magnetics designed for these frequencies almost always feature air cores, indicating significant potential for improved performance by adopting magnetic materials in these applications.

Appendix A
Inductor Optimization Strategy

As described in Section IV, optimized inductors were built to test the validity of the analysis. Magnetic materials were chosen based on their performance factors at the frequencies of interest (10, 30, and 60 MHz). At each frequency, 10 and 100 Ω inductors were built (with the exception of Commercially available toroidal cores were purchased and their dimensions were run through an optimization script, as described below, and shown in the presented flowchart. Given the dimensions of a commercially available magnetic core, the magnetic material's properties, operating frequency, and target inductance, an optimized inductor design was created.

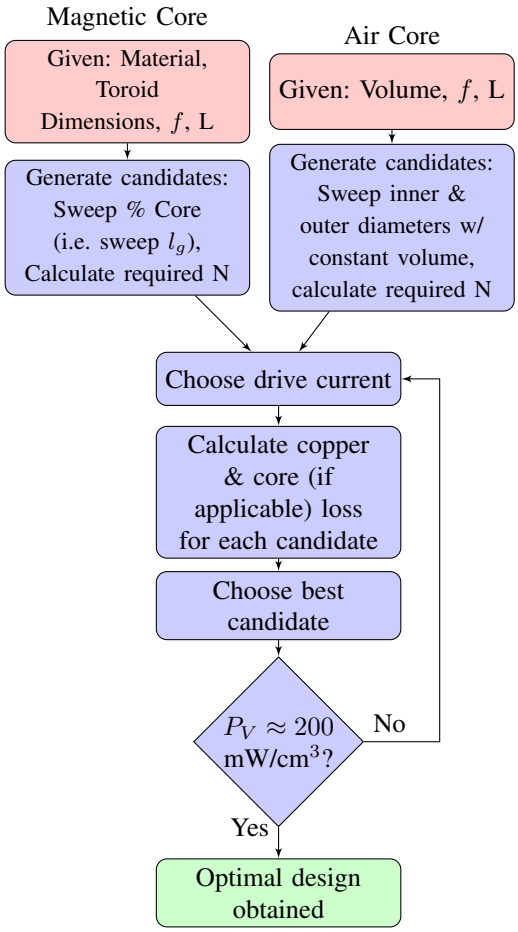

Following the analysis presented in Section II-B, the 'percent core' of the inductor was swept - this method of changing the gap guaranteed constant volume. For each option, turn count was calculated to reach target inductance. Turns were assumed to be foil turns that fully utilized the surface area of the toroid for conduction. A drive current was selected arbitrarily, core & copper losses were then calculated for each option. The option with minimum loss was then checked for its estimated loss density. Our analysis used a figure of 200 mW/cm^3, so we targeted this figure for the optimized loss density. If the selected candidate design's P_V was far from 200 mW/cm^3, a new current was chosen and the process was repeated until an optimized inductor with the correct loss density was produced. Note, however, that the final result was relatively insensitive to drive current, often only shifting by a few percent (in core material composition ratio) depending on what drive current was selected.

Once magnetic cored inductors were designed, the process was repeated with air-core inductors. For each cored inductor, an air-core counterpart with identical volume, operating frequency, and inductance was built. The optimization process was largely similar, except because only volume (and not toroid dimensions) was fixed, the shape of the toroid could be varied. A variety of target candidates were generated by

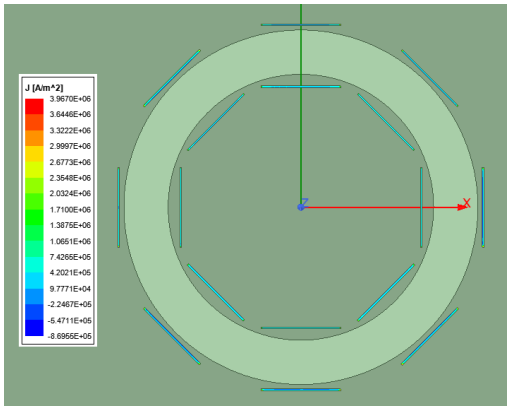

(a) FEA Simulation of foil wound inductor.

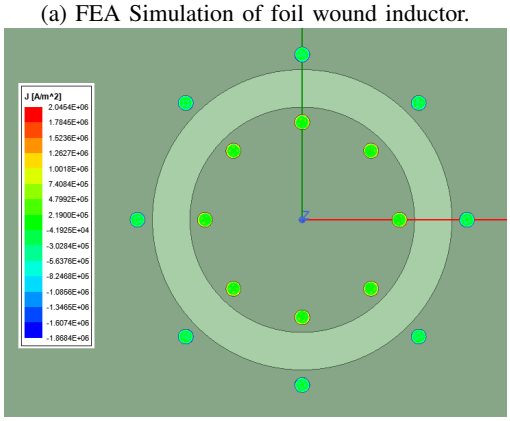

(b) FEA Simulation of traditional wire wound inductor.

Fig. 6: FEA Simulations of two identical inductors with varying winding styles. Note the lower peak current density in the round wire case.

sweeping outer & inner diameters of a cylindrical toroid while holding volume constant. Again, in each case the number of turns was calculated to reach the target inductance, and were treated as perfectly distributed foil conductors. The same optimization point was ran from this point on, and the optimized design was then 3D printed, wound, and tested.

Appendix B
Choice of Foil vs. Round Windings

The analysis presented in Appendix A assumes full utilization of toroid surface area by the use of foil windings. However, the final tested inductors used in this article utilized traditional round wires (using either the largest wire gauge geometrically possible or readily available). This may seem like a willful sacrifice of performance for winding convenience, but that is not the case. When tested, inductors wound with round wire regularly outperformed their foil wound counterparts with the same core and number of turns. We aim to briefly explain this phenomenon and justify this design choice.

It is well understood that the main issues of concern for conduction at high frequencies are the skin and proximity effects, which, if not planned for, can cause copper losses

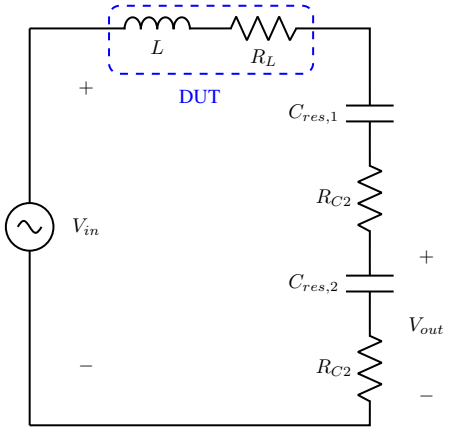

Fig. 7: Schematic of the inductor quality factor measurement setup.

to balloon. A foil winding aims to mitigate these effects by presenting a long and flat cross-section (ostensibly with a thickness greater than a skin depth at the target operating frequency) for current to conduct. However, if current does not flow on the long axis of the foil winding, but instead crowds on its edges, loss can be significantly greater than expected. We posit that within a toroidal inductor, proximity effects cause exactly this phenomenon to occur.

Figure 6 shows two finite element simulations of toroidal inductors with identical cores and number of turns. Despite greater utilization of core surface area, the foil wound case has peak current density and total copper loss 94% and 31.5% higher, respectively, than its round wire counterpart. This indicates that even in cases where proximity effects are often ignored, like that of the foil winding around an inductor, current crowding due to them can significantly increase loss. As such, all of our inductors utilized round wire windings to minimize loss and maximize Q.

Appendix C
Inductor Quality Factor Testing Setup

A series resonant circuit, shown in Fig. 7, was used to measure the quality factor of the inductors built in Section IV. Such an approach has been used to characterize magnetic materials and high quality factor inductors [10], [28]. The method works by resonating the inductor under test with a capacitance, then exciting the circuit at the resonant frequency with a power amplifier. At the resonant frequency, the ratio between V_{out} and V_{in} is directly proportional to the quality factor of the tested inductor. For high quality factor structures or high frequency measurements, it may be necessary to use a capacitor divider as shown to mitigate the effect of probe capacitance. A full derivation of the quality factor expression is shown in [28].

$$Q = \frac{\omega L}{\frac{V_{in}}{V_{out}}\sqrt{R_{C2}^2 + \frac{1}{\omega C_{res,2}^2}^2} - R_{C1} - R_{C2}} \tag{17}$$

REFERENCES

[1] J. Reinert, A. Brockmeyer, and R. De Doncker, "Calculation of losses in ferro- and ferrimagnetic materials based on the modified steinmetz equation," *IEEE Transactions on Industry Applications*, vol. 37, no. 4, pp. 1055–1061, 2001.

[2] K. Venkatachalam, C. Sullivan, T. Abdallah, and H. Tacca, "Accurate prediction of ferrite core loss with nonsinusoidal waveforms using only steinmetz parameters," in *2002 IEEE Workshop on Computers in Power Electronics, 2002. Proceedings.*, 2002, pp. 36–41.

[3] J. Muhlethaler, J. Biela, J. W. Kolar, and A. Ecklebe, "Improved core-loss calculation for magnetic components employed in power electronic systems," *IEEE Transactions on Power Electronics*, vol. 27, no. 2, pp. 964–973, 2012.

[4] G. Zulauf and J. M. Rivas-Davila, "Single-turn air-core coils for high-frequency inductive wireless power transfer," *IEEE Transactions on Power Electronics*, vol. 35, no. 3, pp. 2917–2932, 2020.

[5] P. Hazucha, G. Schrom, J. Hahn, B. Bloechel, P. Hack, G. Dermer, S. Narendra, D. Gardner, T. Karnik, V. De, and S. Borkar, "A 233-mhz 80four-phase dc-dc converter utilizing air-core inductors on package," *IEEE Journal of Solid-State Circuits*, vol. 40, no. 4, pp. 838–845, 2005.

[6] C. R. Sullivan, W. Li, S. Prabhakaran, and S. Lu, "Design and fabrication of low-loss toroidal air-core inductors," in *2007 IEEE Power Electronics Specialists Conference*, 2007, pp. 1754–1759.

[7] C. D. Meyer, S. S. Bedair, B. C. Morgan, and D. P. Arnold, "High-inductance-density, air-core, power inductors, and transformers designed for operation at 100–500 mhz," *IEEE Transactions on Magnetics*, vol. 46, no. 6, pp. 2236–2239, 2010.

[8] C. R. Sullivan, D. V. Harburg, J. Qiu, C. G. Levey, and D. Yao, "Integrating magnetics for on-chip power: A perspective," *IEEE Transactions on Power Electronics*, vol. 28, no. 9, pp. 4342–4353, 2013.

[9] A. J. Hanson, J. A. Belk, S. Lim, C. R. Sullivan, and D. J. Perreault, "Measurements and performance factor comparisons of magnetic materials at high frequency," *IEEE Transactions on Power Electronics*, vol. 31, no. 11, pp. 7909–7925, 2016.

[10] Y. Han, G. Cheung, A. Li, C. R. Sullivan, and D. J. Perreault, "Evaluation of magnetic materials for very high frequency applications," *IEEE Transactions on Power Electronics*, pp. 425–435, 2008.

[11] S. Sinha, A. Kumar, S. Pervaiz, B. Regensburger, and K. K. Afridi, "Design of efficient matching networks for capacitive wireless power transfer systems," in *2016 IEEE 17th Workshop on Control and Modeling for Power Electronics (COMPEL)*, 2016, pp. 1–7.

[12] S. Liu, M. Liu, S. Yang, C. Ma, and X. Zhu, "A novel design methodology for high-efficiency current-mode and voltage-mode class-e power amplifiers in wireless power transfer systems," *IEEE Transactions on Power Electronics*, vol. 32, no. 6, pp. 4514–4523, 2017.

[13] Y. Lu and W.-H. Ki, "A 13.56 mhz cmos active rectifier with switched-offset and compensated biasing for biomedical wireless power transfer systems," *IEEE Transactions on Biomedical Circuits and Systems*, vol. 8, no. 3, pp. 334–344, 2014.

[14] T. C. Beh, M. Kato, T. Imura, S. Oh, and Y. Hori, "Automated impedance matching system for robust wireless power transfer via magnetic resonance coupling," *IEEE Transactions on Industrial Electronics*, vol. 60, no. 9, pp. 3689–3698, 2013.

[15] S. Aldhaher, D. C. Yates, and P. D. Mitcheson, "Design and development of a class ef_2 inverter and rectifier for multimegahertz wireless power transfer systems," *IEEE Transactions on Power Electronics*, vol. 31, no. 12, pp. 8138–8150, 2016.

[16] P. Piyasena, C. Dussault, T. Koutchma, H. S. Ramaswamy, and G. B. Awuah, "Radio frequency heating of foods: Principles, applications and related properties—a review," *Critical Reviews in Food Science and Nutrition*, vol. 43, no. 6, pp. 587–606, 2003, pMID: 14669879. [Online]. Available: https://doi.org/10.1080/10408690390251129

[17] M. Network, S. Sinha, Y. Hou, D. Ni, Q. Ji, A. Persaud, P. Seidl, T. Schenkel, A. Lal, and K. K. Afridi, "A 27.12-mhz 10-kv power amplifier for compact particle accelerators utilizing an optimized," in *2020 IEEE Energy Conversion Congress and Exposition (ECCE)*, 2020, pp. 5452–5457.

[18] S. Aldhaher, D. C. Yates, and P. D. Mitcheson, "Modeling and analysis of class ef and class e/f inverters with series-tuned resonant networks," *IEEE Transactions on Power Electronics*, vol. 31, no. 5, pp. 3415–3430, 2016.

[19] L. Raymond, W. Liang, J. Choi, and J. Rivas, "27.12 mhz large voltage gain resonant converter with low voltage stress," in *2013 IEEE Energy Conversion Congress and Exposition*, 2013, pp. 1814–1821.

[20] L. Roslaniec, A. S. Jurkov, A. A. Bastami, and D. J. Perreault, "Design of single-switch inverters for variable resistance/load modulation operation," *IEEE Transactions on Power Electronics*, vol. 30, no. 6, pp. 3200–3214, 2015.

[21] J. M. Rivas, Y. Han, O. Leitermann, A. D. Sagneri, and D. J. Perreault, "A high-frequency resonant inverter topology with low-voltage stress," *IEEE Transactions on Power Electronics*, vol. 23, no. 4, pp. 1759–1771, 2008.

[22] A. Clements, V. Vishnoi, S. Dehghani, and T. Johnson, "A comparison of gan class e inverter and synchronous rectifier designs for 13.56 mhz, 27.12 mhz and 40.68 mhz ism bands," in *2018 IEEE Wireless Power Transfer Conference (WPTC)*, 2018, pp. 1–4.

[23] R. S. Bayliss III, R. S. Yang, A. J. Hanson, C. R. Sullivan, and D. J. Perreault, "Design, implementation, and evaluation of high-efficiency high-power radio-frequency inductors," in *2021 IEEE Applied Power Electronics Conference and Exposition (APEC)*, 2021.

[24] A. L. F. Stein, P. A. Kyaw, and C. R. Sullivan, "Wireless power transfer utilizing a high-q self-resonant structure," *IEEE Transactions on Power Electronics*, vol. 34, no. 7, pp. 6722–6735, 2019.

[25] D. W. Lee, K.-P. Hwang, and S. X. Wang, "Fabrication and analysis of high-performance integrated solenoid inductor with magnetic core," *IEEE Transactions on Magnetics*, vol. 44, no. 11, pp. 4089–4095, 2008.

[26] D. J. Perreault, C. R. Sullivan, R. S. Yang, R. Bayliss, and A. J. Hanson, "Self-shielded high frequency inductor," United States Application Patent 63/150,704, 2021.

[27] J. Hu and C. Sullivan, "The quasi-distributed gap technique for planar inductors: design guidelines," in *IAS '97. Conference Record of the 1997 IEEE Industry Applications Conference Thirty-Second IAS Annual Meeting*, vol. 2, 1997, pp. 1147–1152 vol.2.

[28] R. S. Yang, A. J. Hanson, B. A. Reese, C. R. Sullivan, and D. J. Perreault, "A low-loss inductor structure and design guidelines for high-frequency applications," *IEEE Transactions on Power Electronics*, vol. 34, no. 10, pp. 9993–10 005, 2019.